Theoretical Investigation on H-Abstraction Reactions of Silanes with H and CH$_3$ Attacking: A Comparative Study with Alkane Counterparts

Qilong Fang, Yan Zhang, Jingxian Xia, and Yuyang Li*

Read Online

ACCESS | Metrics & More | Article Recommendations | SI Supporting Information

ABSTRACT: Silicon-based organic precursors are widely applied in the vapor-fed flame synthesis of monocrystalline silicon, silicon dioxide, and silicon nitride. Due to the lack of kinetic investigations on reactions of silicon-based organic precursors, rate constants were usually analogized to those of their hydrocarbon counterparts. Investigations on the similarities and differences between the two types of compounds become necessary. This work reports a comparative theoretical investigation on H-abstraction reactions with H and CH$_3$ attacking for silanes and their alkane counterparts, including silane and methane, disilane, methylsilane and ethane, dimethylsilane and propane, trimethylsilane and *iso*-butane, and tetramethylsilane and *neo*-pentane at the domain-based local pair natural orbital coupled cluster with perturbative triple excitations (DLPNO-CCSD(T))/cc-pVTZ//M06−2X/cc-pVTZ level. The rate

constants were calculated using the conventional transition-state theory coupled with the asymmetric Eckart tunneling corrections over 600−2000 K. The calculated results show that dramatic discrepancies exist between H-abstraction from silicon sites in silanes and equivalent carbon sites in their alkane counterparts with H and CH$_3$ attacking. The H-abstraction reactions from the primary carbon sites in silanes have generally lower barrier energies than the similar reactions in their alkane counterparts, while those in methylsilane and dimethylsilane with H attacking are the only two with higher barrier energies. Electrostatic potential mapped molecular van der Waals surfaces were adopted to provide insight into the calculated trends in barrier energies. The H-abstraction reactions from silicon sites in silanes have much higher rate constants than those from equivalent carbon sites in their alkane counterparts, especially under low-temperature conditions, while the rate constants of H-abstraction reactions from primary carbon sites in silanes and their alkane counterparts show relatively strong analogy.
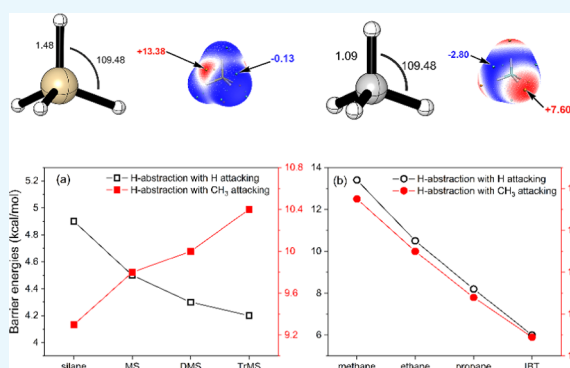
1. INTRODUCTION

In the field of nanomaterial synthesis, great attention is paid to the applications of flame synthesis methods.[1−5] Among flame synthesis methods, vapor-fed aerosol flame synthesis (VAFS) can facilitate direct growth of nanomaterials and has a simple preparation process compared with wet chemical methods such as coprecipitation and a sol−gel method,[6] making it a promising nanomaterial synthesis method. As a result, VAFS technology has been widely applied in industrial production of nano-particles, such as gaseous silica, titanium dioxide pigment, and carbon black.[7] In particular, many studies have been carried out on the VAFS of silicon-containing nanoparticles, such as silicon carbide, silicon nitride, and silicon dioxide, which are widely used in semiconductor, electronic industry, biomedical and other fields,[8−10] where silanes are important VAFS precursors.

For better control of the particle sizes, chemical activities, and other properties of silicon-containing nanoparticles, under-standing the reaction mechanisms and developing kinetic models of silanes under combustion circumstances are essential.[11,12] Britten et al.[13] developed a kinetic model of silane

(SiH$_4$) to describe the combustion characteristics under a wide range of conditions, while Miller et al.[14] updated the Britten model using their calculated rate constants of SiH$_3$ + O$_2$ reactions. Parandaman et al.[15] studied the kinetics of the thermal decomposition of tetramethylsilane (TeMS, Si(CH$_3$)$_4$) behind the reflected shock waves and developed a pyrolysis model of TeMS. Sela et al.[16] investigated the TeMS decomposition in a shock tube using gas chromatography/ mass spectrometry (GC/MS) and high-repetition-rate time-of-flight mass spectrometry (HRR-TOF-MS). They also developed a new TeMS submechanism and incorporated it into the USC Mech II model to predict their measurements. Janbazi et al.[17]
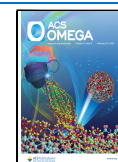
developed an oxidation model of TeMS to simulate their measured results in a low-pressure lean H_2/TeMS/O_2/Ar flame.

The most important parameters in kinetic models are rate constants of elementary reactions, especially for the H-abstraction reactions, which play an important role in combustion of VAFS precursors.[17,18] However, the rate constants of silicon-containing reactions are far from sufficiently understood, especially compared with those of their hydrocarbon counterparts. Mick et al.[19] obtained the rate constant of $Si_2H_6 = SiH_4 + SiH_2$ by the SiH_2 absorption measurements in a shock tube over 0.35−1.3 bar and 1070−1381 K. Hershberger and co-workers[20,21] measured the rate constants of silyl radical (SiH_3) with NO_2, O_2, and H_2O_2 by time-resolved infrared diode laser absorption spectroscopy over 235−573 K at low pressure. Ding and Marshall[22] measured the rate constants of the reactions of Cl and Br with trimethylsilane (TrMS, $(CH_3)_3SiH$) using a flash-photolysis resonance fluorescence (FPRF) method over 300−460 K at low pressure. For theoretical calculations, Espinosa-Garcia et al.[23] calculated the rate constants of the $SiH_4 + H = SiH_3 + H_2$ reaction and investigated the kinetic isotope effect. Wu et al.[24] calculated the rate constants for the reactions of $SiH_4 + H$ and $Si_2H_6 + H_2$. Qi and Sun[25] also studied the reaction paths and rate constants of $SiH_4 + H$ using the *ab initio* method. Oueslati et al.[26] conducted *ab initio* calculations on the H-abstraction reactions of TeMS with H and D attacking.

To incorporate silicon-containing reactions without available rate constants in kinetic models, analogy with their hydrocarbon counterparts or model hydrocarbon compounds becomes a practical approach and has been widely adopted in the development of kinetic models for silicon-based precursors.[17,27−29] Here comes an important question: is it reasonable and always reliable to refer the rate constants of silicon-containing reactions to those of their hydrocarbon counterparts or model hydrocarbon compounds, even if silicon and carbon belong to the same element family? Several pioneering studies have been performed in this field. Peukert et al.[30] measured the rate constant for H-abstraction from TeMS and *neo*-pentane (NPT, $C(CH_3)_4$) with H attacking in a shock tube combined with time-resolved H-atom resonance absorption spectrometry (H-ARAS) and found that their rate constants are similar. They also compared the H-abstraction reaction between tetramethoxysilane (TMOS, $Si(OCH_3)_4$) and dimethyl ether (DME, CH_3OCH_3) and also found that TMOS has similar rate constants to DME over 1111−1238 K at 1.3−1.4 bar.[31] Nurkowski et al.[32] calculated the rate constants for pressure-dependent reactions $(OH)_3SiOC_2H_5 = (OH)_3SiOCH_2 + CH_3$ and $C_2H_5OH = CH_2OH + CH_3$ using variable reaction coordinate variational transition-state theory (VRC-TST), which showed comparable rate constants between the two reactions. They also calculated the ethylene elimination reaction of TEOS and found that the rate constant is similar to that of the H_2O elimination reaction of ethanol.[21] However, these studies are only focused on limited systems and the comparison is usually insufficient, especially for the silane systems. No specific investigation has been performed on the influence of different molecular structures and attacking radicals, as well as the behaviors between silicon and carbon sites.

In this work, the H-abstraction reactions from six cases of silanes and their alkane counterparts, including silane and methane (CH_4), disilane (Si_2H_6) and ethane (C_2H_6), methylsilane (CH_3SiH_3) and ethane, dimethylsilane (DMS, $(CH_3)_2SiH_2$) and propane (C_3H_8), TrMS and *iso*-butane (IBT,

$(CH_3)_3CH$), and TeMS and NPT, were theoretically investigated. Among them, the H-abstraction reactions of DMS and TrMS systems were studied for the first time. Table 1 lists the

Table 1. List of Abbreviations, and Corresponding Species and Their Chemical Formulas

| species	chemical formula	abbreviation
dimethylsilane	$(CH_3)_2SiH_2$	DMS
trimethylsilane	$(CH_3)_3SiH$	TrMS
tetramethylsilane	$Si(OCH_3)_4$	TeMS
iso-butane	$(CH_3)_3CH$	IBT
neo-pentane	$C(CH_3)_4$	NPT

abbreviations and corresponding species and their chemical formulas. The first five cases can help explore the behaviors between silicon and carbon sites, while the comparison between methylsilanes and their alkane counterparts can help investigate the influence of different molecular structures on the primary carbon site. On the other hand, most of the VAFS systems adopt H_2 and methane flames as the base flames, which will lead to a combustion circumstance with abundant H and CH_3 radicals. Thus, H and CH_3 were selected as the two attacking radicals in this work to reveal the influence of different attacking radicals. Potential energy surfaces (PESs) and electrostatic potential (ESP) mapped molecular van der Waals (vdW) surfaces were explored and rate constants were calculated, which provide insight into differences and similarities between H-abstraction reactions from silanes and their alkane counterparts.

2. RESULTS AND DISCUSSIONS

2.1. Barrier Energies of H-Abstraction from Silanes and Alkanes.
The calculated barrier energies with zero-point energy (ZPE) correction for H-abstraction from silanes and their alkane counterparts are shown in Figure 1 with H and CH_3 as the attacking radicals, respectively. The PESs, relative enthalpies (ΔH), free energies (ΔG), and entropies (ΔS) of the H-abstraction transition states at different temperatures, and geometries and frequencies of species are listed in the
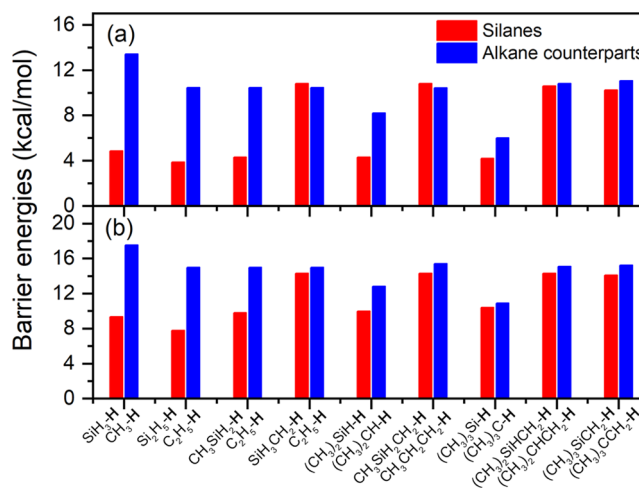
Figure 1. Calculated barrier energies with ZPE corrected for H-abstraction from silanes and alkanes with (a) H attacking and (b) CH_3 attacking at the domain-based local pair natural orbital coupled cluster with perturbative triple excitations (DLPNO-CCSD(T))/cc-pVTZ// M06−2X/cc-pVTZ level.
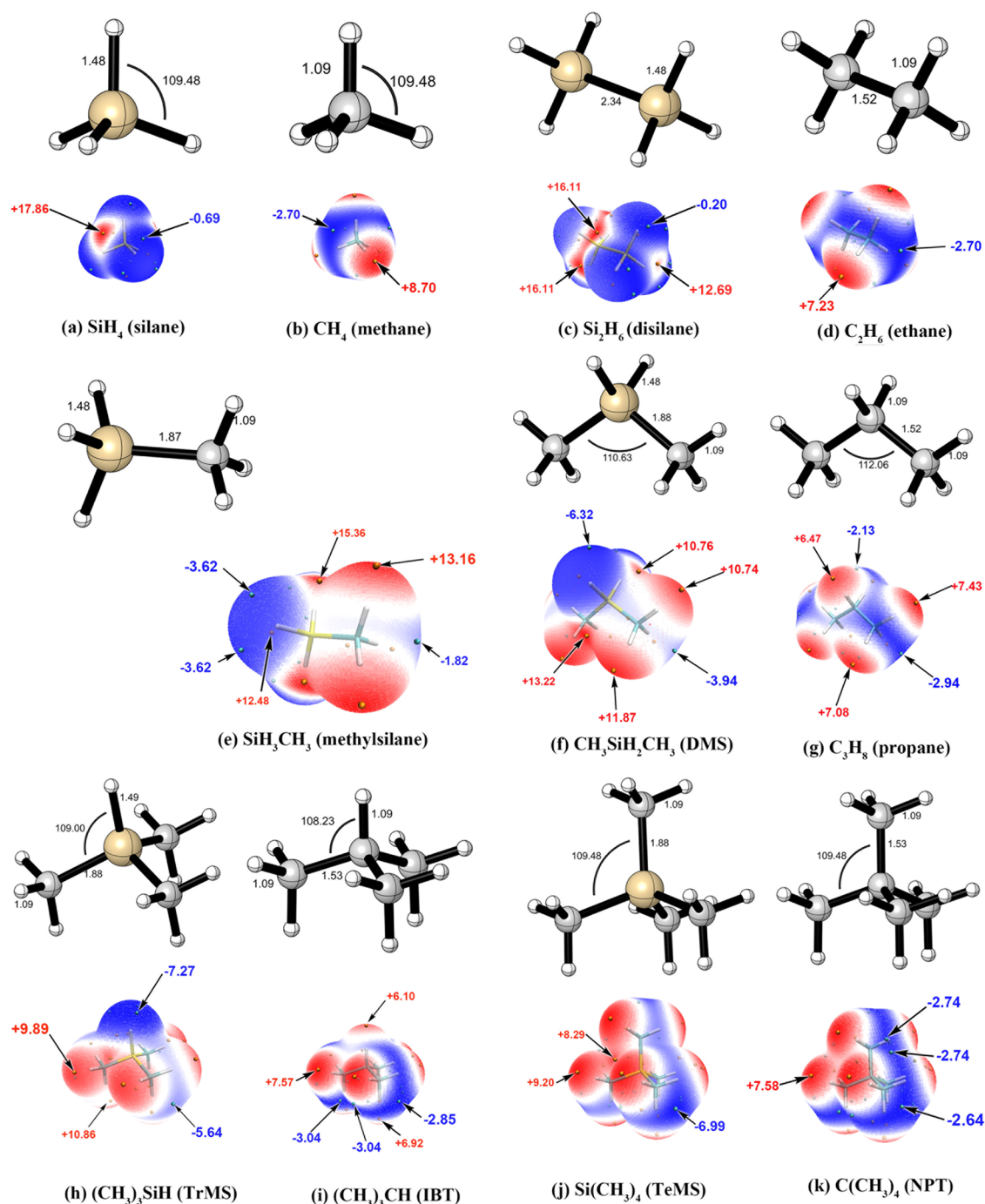
Figure 2. Configurations and ESP-mapped molecular vdW surfaces of silanes and their alkane counterparts with the unit in kcal/mol. Red and blue colors denote positive and negative ESP values, respectively, with the transition regions shown in white. Surface local minima and maxima of ESP are represented as small cyan and orange spheres, respectively. The color scale bar is different for each molecule.

Supporting Information. The configurations and ESP-mapped vdW surfaces along with surface extrema of silanes and alkanes are shown in Figure 2.

For silane and methane, the barrier energies of H-abstraction from silane and methane are 4.9 and 13.4 kcal/mol with H attacking, while the values become 9.3 and 17.5 kcal/mol with CH_3 attacking, respectively, as shown in Figure 1. The barrier energies for H-abstraction from silane with H and CH_3 attacking are lower than those of H-abstraction from methane, which is in accordance with the order of Si−H and C−H bond dissociation energies (BDEs) in silane (91.7 kcal/mol) and methane (105.0

kcal/mol).[33] From the ESP-mapped molecular vdW surface of silane shown in Figure 2a, the global maximum on the SiH_4 surface is found to be +17.86 kcal/mol, and the positive region is mainly localized on the silicon atom. The global minima on the surface are found to be −0.69 kcal/mol, which concentrate on the hydrogen atoms. For the ESP-mapped molecular vdW surface of methane shown in Figure 2b, the global maxima on the CH_4 surface are found to be +8.70 kcal/mol, and the positive regions are localized on the hydrogen atoms. The global minima (−2.70 kcal/mol) are located on the carbon atom. The great difference between silane and methane is caused by the fact that
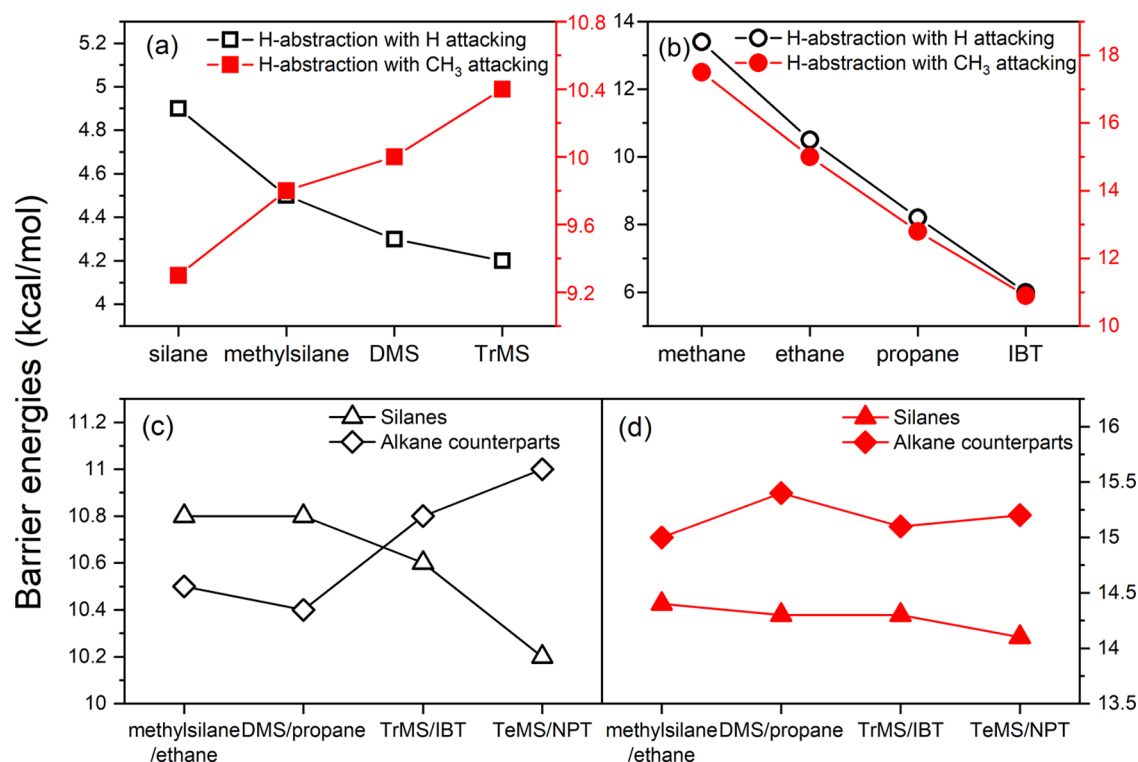
Figure 3. Calculated barrier energies with ZPE corrected for H-abstraction reactions from (a) silicon sites in silanes (square) and (b) equivalent carbon sites in their alkane counterparts (circle) with H attacking (hollow) and CH_3 attacking (solid), and from the primary carbon sites in silanes (triangle) and their alkane counterparts (diamond) with (c) H attacking (hollow) and (d) CH_3 attacking (solid).

the electronegativities of the silicon atom, carbon atom, and hydrogen atom are 1.90, 2.55, and 2.20, respectively. Hence, the bonding pairs in the Si−H bonds of silane are biased toward the hydrogen atoms, while the bonding pairs in the C−H bonds of methane are biased toward the carbon atom. This results in observation that the positive regions are localized on the silicon atom in silane and the hydrogen atoms in methane. It is concluded that silane and methane have dramatically different distributions of reactive regions and the BDE of the Si−H bond is weaker than that of the C−H bond in methane. Besides, silane has a larger nucleophilic region. These reasons result in the lower barrier energies of H-abstraction reactions from silane.

For disilane, Wu et al.[24] found that its reaction with H has three pathways, which is a special feature of disilane compared with ethane. In this work, only the H-abstraction pathway was investigated. The barrier energies of H-abstraction reactions from disilane and ethane are 3.9 and 10.5 kcal/mol with H attacking and 7.8 and 15.0 kcal/mol with CH_3 attacking, respectively, showing the same trends as the case of silane and methane. The lower barrier energies of disilane than ethane are also in accordance with the order of Si−H and C−H BDEs in disilane and ethane.[33] Similar to the case of silane and methane, Figure 2c,d shows that the local electrophilic capacities on the hydrogen atoms of disilane are weaker than those of ethane, which are strongly correlated with the lower barrier energy of H-abstraction from disilane.

Methylsilane has two types of heavy-atom sites for H-abstraction, *i.e.*, the primary carbon site and the primary silicon site. Figure 1 shows that the barrier energies of H-abstraction from the primary silicon site in methylsilane are 4.5 and 9.8 kcal/mol with H and CH_3 attacking, respectively, which are much lower than those on the primary carbon site in ethane (10.5 and 15.0 kcal/mol). Compared with the H-abstraction from the

primary silicon site in disilane, the barrier energies of H-abstraction from the primary silicon site in methylsilane are higher, which are the same as the trend in BDEs of disilane (89.1 kcal/mol[33]) and methylsilane (92.7 kcal/mol[33]). As seen from Figure 1, it is interesting to find that the barrier energy of H-abstraction from the primary carbon site in methylsilane with H attacking is higher than H-abstraction from ethane, while the order is opposite for H-abstraction with CH_3 attacking. This phenomenon will be discussed in detail in the next paragraph together with the case in DMS and propane.

For DMS and propene, the barrier energies of H-abstraction reactions from the secondary silicon site in DMS and the secondary carbon site in propane are 4.3 and 8.2 kcal/mol with H attacking and 10.0 and 12.8 kcal/mol with CH_3 attacking, respectively. The lower barrier energies of H-abstraction reactions from the silicon site than those from the equivalent carbon site are in accordance with the cases of silane and methane, disilane and ethane, and methylsilane and ethane. As seen from Figure 1, the barrier energies of H-abstraction reactions from the primary carbon sites in DMS and propane are 10.8 and 10.4 kcal/mol with H attacking and 14.3 and 15.4 kcal/mol with CH_3 attacking, respectively, showing the same trends as those in methylsilane and ethane. But it should be emphasized among all 32 H-abstraction reactions in this work, and the reactions from the primary carbon sites in methylsilane and DMS with H attacking are the only two with higher barrier energies than the similar reactions in their alkane counterparts. As seen from Figure 2d−g, it can be observed that both methylsilane and DMS have relatively large and strong electron-affinitive regions in the primary carbon sites and small electronegative regions, compared with their alkane counterparts. Due to the uniform electron-affinitive configuration of the H atom, the H attacking on the primary carbon sites in

Table 2. Arrhenius Fit Parameters of Rate Constants (A, n, and E_a) per H Atom for the Investigated Reactions[a]

| no.	reactions	A	n	E_a
1	$SiH_4 + H = SiH_3 + H_2$	4.878×10^6	2.224	2791.7
2	$SiH_4 + CH_3 = SiH_3 + CH_4$	8.526×10^{-1}	3.952	5712.9
3	$CH_4 + H = CH_3 + H_2$	1.998×10^3	3.110	9135.0
4	$CH_4 + CH_3 = CH_3 + CH_4$	1.061×10^{-3}	4.595	12041.0
5	$Si_2H_6 + H = Si_2H_5 + H_2$	4.426×10^7	1.987	2547.8
6	$Si_2H_6 + CH_3 = Si_2H_5 + CH_4$	3.859×10^0	3.753	4815.1
7	$C_2H_6 + H = C_2H_5 + H_2$	9.188×10^3	2.950	6765.7
8	$C_2H_6 + CH_3 = C_2H_5 + CH_4$	9.727×10^{-4}	4.663	9698.6
9	$CH_3SiH_3 + H = CH_2SiH_3 + H_2$	1.150×10^5	2.666	7588.2
10	$CH_3SiH_3 + CH_3 = CH_2SiH_3 + CH_3$	1.290×10^1	4.027	10348.0
11	$CH_3SiH_3 + H = CH_3SiH_2 + H_2$	2.280×10^7	2.072	2990.7
12	$CH_3SiH_3 + CH_3 = CH_3SiH_2 + CH_3$	2.726×10^0	3.700	6754.5
13	$(CH_3)_2SiH_2 + H = CH_3SiH_2CH_2 + H_2$	5.389×10^3	3.008	6838.7
14	$(CH_3)_2SiH_2 + CH_3 = CH_3SiH_2CH_2 + CH_4$	1.716×10^{-2}	4.393	9629.7
15	$(CH_3)_2SiH_2 + H = CH_3SiHCH_3 + H_2$	1.808×10^7	2.118	2817.1
16	$(CH_3)_2SiH_2 + CH_3 = CH_3SiHCH_2 + CH_4$	4.518×10^1	3.489	7192.2
17	$C_3H_8 + H = nC_3H_7 + H_2$	8.637×10^3	3.015	6798.2
18	$C_3H_8 + CH_3 = nC_3H_7 + CH_4$	2.884×10^4	4.583	10160.0
19	$C_3H_8 + H = iC_3H_7 + H_2$	2.836×10^4	2.787	4910.2
20	$C_3H_8 + CH_3 = iC_3H_7 + CH_4$	2.601×10^{-3}	4.549	7923.0
21	$(CH_3)_3SiH + H = (CH_3)_2SiHCH_2 + H_2$	1.260×10^5	2.595	7380.2
22	$(CH_3)_3SiH + CH_3 = (CH_3)_2SiHCH_2 + CH_3$	3.860×10^{-2}	4.008	10199
23	$(CH_3)_3SiH + H = (CH_3)_3Si + H_2$	4.590×10^7	2.040	2856.8
24	$(CH_3)_3SiH + CH_3 = (CH_3)_3Si + CH_3$	1.281×10^1	3.621	7756.7
25	$(CH_3)_3CH + H = (CH_3)_2CHCH_2 + H_2$	1.390×10^5	2.596	7844.7
26	$(CH_3)_3CH + CH_3 = (CH_3)_2CHCH_2 + CH_3$		4.646	9836.8
27	$(CH_3)_3CH + H = (CH_3)_3C + H_2$	4.300×10^5	2.528	3487.7
28	$(CH_3)_3CH + CH_3 = (CH_3)_3C + CH_3$	2.191×10^{-1}	4.023	7309.9
29	$Si(CH_3)_4 + H = Si(CH_3)_3CH_2 + H_2$	9.851×10^3	2.911	6485.2
30	$Si(CH_3)_4 + CH_3 = Si(CH_3)_3CH_2 + CH_4$	2.363×10^{-3}	4.394	9336.9
31	$C(CH_3)_4 + H = C(CH_3)_3CH_2 + H_2$	9.244×10^3	2.886	7432.9
32	$C(CH_3)_4 + CH_3 = C(CH_3)_3CH_2 + CH_4$	2.087×10^{-4}	4.649	9994.3

[a]Units are cm^3, mol, s, cal.

methylsilane and DMS becomes relatively difficult than that in ethane and propane, respectively. In contrast, CH_3 attacking is less affected because of the central electronegative feature of CH_3 radical shown in Figure S7 in the Supporting Information.

For the H-abstraction from the tertiary silicon site in TrMS, the barrier energies of H-abstraction reactions with H and CH_3 attacking are about 2 and 0.5 kcal/mol lower than those from the tertiary carbon site in IBT, respectively. For the H-abstraction from the primary carbon sites in TrMS and IBT, the barrier energies of H-abstraction reactions from TrMS with H and CH_3 attacking are about 0.2 and 0.8 kcal/mol lower than those from IBT, respectively. Furthermore, the barrier energies of H-abstraction reactions from the primary carbon sites in TeMS and NPT are 10.2 and 14.1 kcal/mol with H attacking and 14.1 and 15.2 kcal/mol with CH_3 attacking, respectively. Different from methylsilane and DMS, TrMS and TeMS have relatively small and weak electron-affinitive regions in the primary carbon sites and strong electronegative regions, compared with their alkane counterparts. As a result, the H-abstraction reactions from the primary carbon sites in TrMS and TeMS have lower barrier energies than the similar reactions in their alkane counterparts, regardless of which radical attacks.

Figure 3 compares the barrier energies for H-abstraction reactions from silicon sites in silanes and equivalent carbon sites in their alkane counterparts and those from the primary carbon sites in silanes and their alkane counterparts, respectively, to better understand the effect of the number of methyl branches. As seen from Figure 3a, the barrier energies of H-abstraction from silicon sites in silanes with H attacking decrease as the number of methyl branches increases, while those with CH_3 attacking have the opposite trend. This is different from the H-abstraction from equivalent carbon sites in their alkane counterparts, as shown in Figure 3b. The BDEs of Si−H bonds are 91.7, 92.7, 93.5, and 94.7 kcal/mol for silane, methylsilane, DMS, and TrMS, respectively, while the BDEs of equivalent C−H bonds are 105.0, 100.5, 98.1, and 95.7 kcal/mol for methane, ethane, propane, and IBT, respectively.[33] Hence, the increase of barrier energies for H-abstraction reactions from silicon sites in silanes with CH_3 attacking and the decrease of barrier energies for H-abstraction reactions from equivalent carbon sites in their alkane counterparts with H and CH_3 attacking, as the number of methyl branches increases, are associated with the trends of corresponding BDEs. As a result, the barrier energy of H-abstraction from the tertiary silicon site in TrMS with CH_3 attacking becomes very close to that from the tertiary carbon site in IBT. It can be found from Figure 2a,e,f,h that the nucleophilic capacity of the H atom on the silicon sites increases with the increasing number of methyl branches, which results in the increasing stability of reactive complexes and consequently lower barrier energies for the H-abstraction from silanes with H attacking. Furthermore, the barrier energies of H-abstraction reactions from the primary carbon sites in both
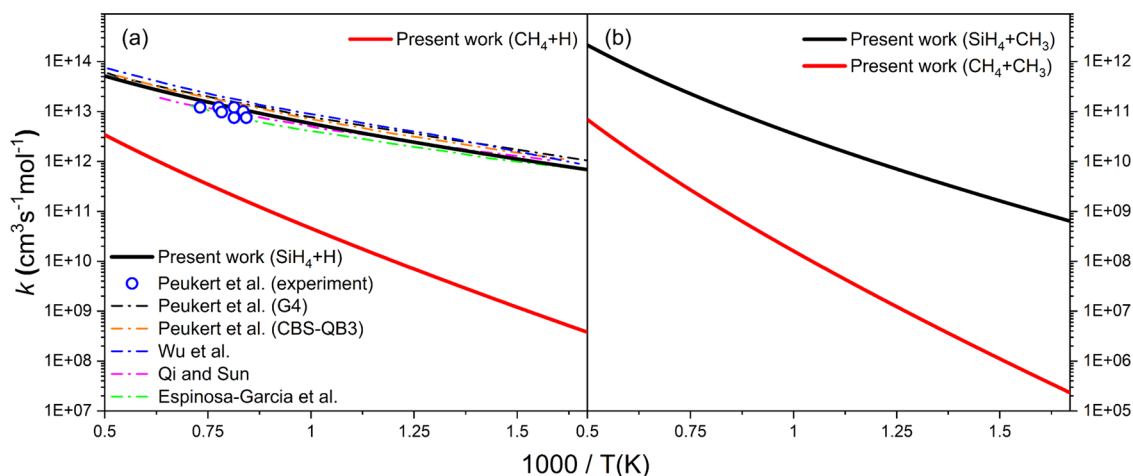
Figure 4. Calculated rate constants of H-abstraction from silane and methane with (a) H attacking and (b) CH_3 attacking at the DLPNO-CCSD(T)/ cc-pVTZ//M06−2X/cc-pVTZ level. Black and red solid lines denote the calculated results of silane and methane in this work, respectively. Blue hollow circle denote the measured results of silane by Peukert et al.[30] Black, orange, blue, purple, and green dashed lines denote calculated rate constants of silane by Peukert et al.[30] at the G4 level, Peukert et al.[30] at the CBS-QB3 level, Wu et al.[24] at the CCSD(T)/6−311++G(3df,2p)// CCSD(T)/6−311+G(d,p) level, Qi and Sun[25] at the G2//QCISD/6−311+G(df, pd) level, and Espinosa-Garcia et al. using the *ab initio* method.[23]
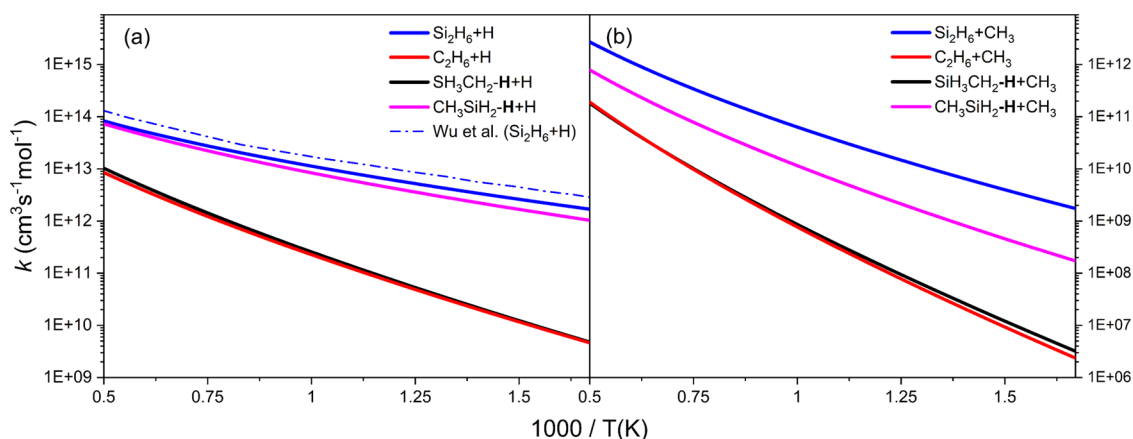
Figure 5. Calculated rate constants of H-abstraction from disilane, methylsilane, and ethane with (a) H attacking and (b) CH_3 attacking at the DLPNO-CCSD(T)/cc-pVTZ//M06−2X/cc-pVTZ level. Black and red solid lines denote the calculated results of disilane and ethane in this work, respectively. Black dashed line denotes the calculated results of disilane by Wu et al.[24] at the CCSD(T)/6−311++G(3df,2p)//CCSD(T)/6− 311+G(d,p) level.

silanes and their alkane counterparts with H and CH_3 attacking have generally less apparent trends, as shown in Figure 3c,d.
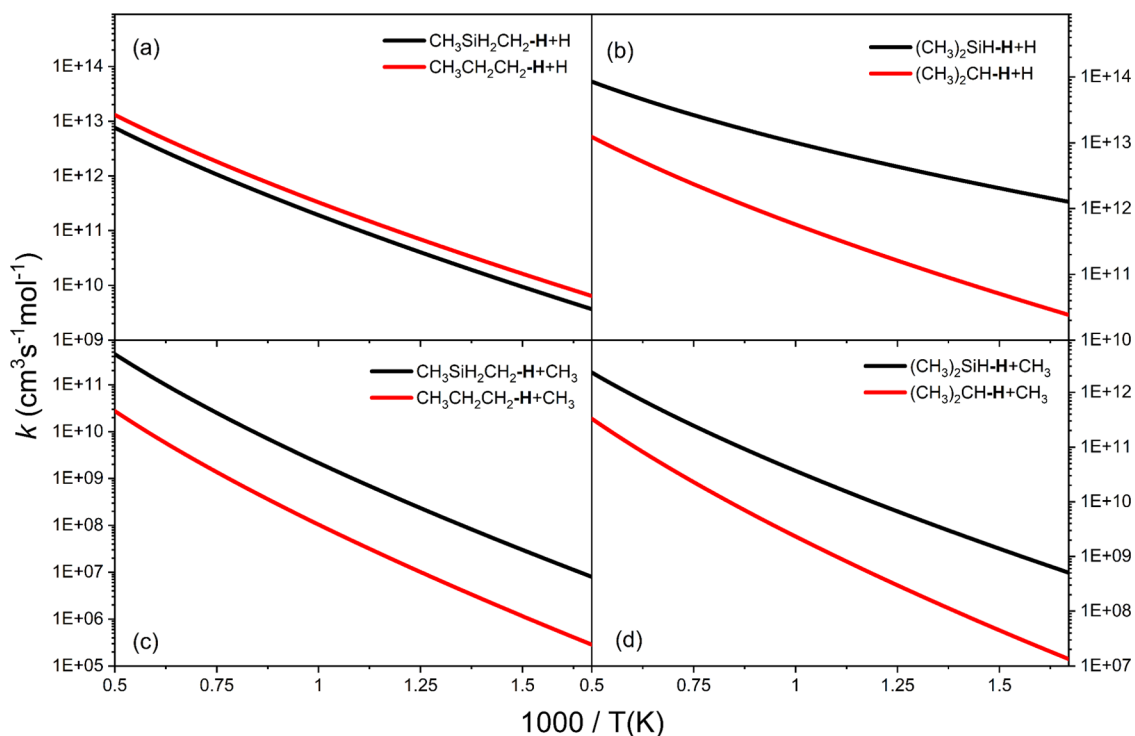
2.2. Rate Constants of H-Abstraction from Silanes and Alkanes. *2.2.1. Silane and Methane.* For the calculated rate constants, the Arrhenius fit parameters (A, n, and E_a) of all investigated reactions are listed in Table 2. The calculated rate constants of H-abstraction reactions from silane and methane with H attacking (R1, R3) and CH_3 attacking (R2, R4) over 600−2000 K are shown in Figure 4. Besides, the calculated rate constants in this work are compared with the experimental and calculated results in the literature. As mentioned above, the rate constant for H-abstraction from silane with H attacking was measured and calculated by many groups, providing more literature results than other silanes. As shown in Figure 4a, the calculated rate constant of R1 in this work is a little lower than those calculated by Peukert et al.[30] and Wu et al.,[24] and a little faster than that calculated by Qi and Sun[25] and Espinosa-Garcia et al.,[23] showing a generally central location in the distribution of available calculated results. Furthermore, the present rate

constant is also very close to the measured results by Peukert et al.[30]

Figure 4 shows huge discrepancies between the rate constants of H-abstraction reactions from silane and methane with either H attacking or CH_3 attacking. The rate constants of H-abstraction reactions from silane with H and CH_3 attacking are much faster than those from methane, which are in good accordance with their lower barrier energies. Strong variations in the ratios of k_1/k_3 and k_2/k_4 over the investigated temperature region can be observed from Figure 4, revealing that the analogy between the H-abstraction reactions from silane and methane is weak. Although the two counterparts have similar configurations, silane is much more active than methane.

2.2.2. Disilane, Methylsilane, and Ethane. Figure 5 shows the calculated rate constants of H-abstraction reactions from disilane, ethane, and methylsilane with H attacking (R5, R7, R9, and R11) and CH_3 attacking (R6, R8, R10, and R12) at the DLPNO-CCSD(T)/cc-pVTZ//M06−2X/cc-pVTZ level. It can be found from Figure 5a that the calculated rate constant of H-abstraction from disilane with H attacking is a little lower

Figure 6. Calculated rate constants of H-abstraction from DMS and propane with (a, b) H attacking and (c, d) CH_3 attacking at the DLPNO-CCSD(T)/cc-pVTZ//M06−2X/cc-pVTZ level. Black and red solid lines denote the calculated results of DMS and propane in this work, respectively.
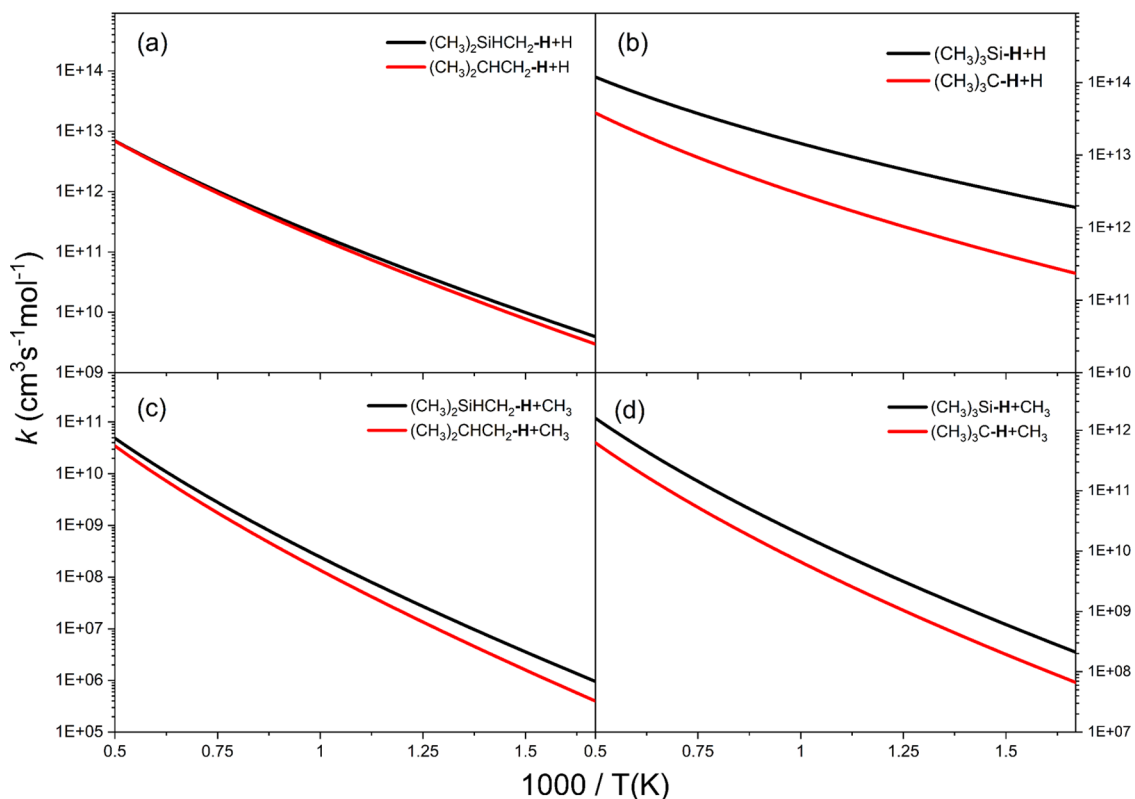
Figure 7. Calculated rate constants of H-abstraction from TrMS and IBT with (a, b) H attacking and (c, d) CH_3 attacking at the DLPNO-CCSD(T)/cc-pVTZ//M06−2X/cc-pVTZ level. Black and red solid lines denote the calculated results of TrMS and IBT in this work, respectively.

than that reported by Wu et al.[24] at the CCSD(T)/6−311++G(3df,2p)//CCSD(T)/6−311+G(d,p) level. Compared to the H-abstraction from the primary carbon site in ethane, the H-abstraction reactions from the primary silicon sites in disilane

and methylsilane are much faster, which is similar to the case of silane and methane. Strong variations in the ratios of k_5/k_7 and k_6/k_8 over the investigated temperature region can be observed from Figure 5, revealing the weak analogy between the H-

Figure 8. Calculated rate constants of H-abstraction reactions from silicon sites in silanes and equivalent carbon sites in their alkane counterparts with (a) H attacking and (b) CH_3 attacking.
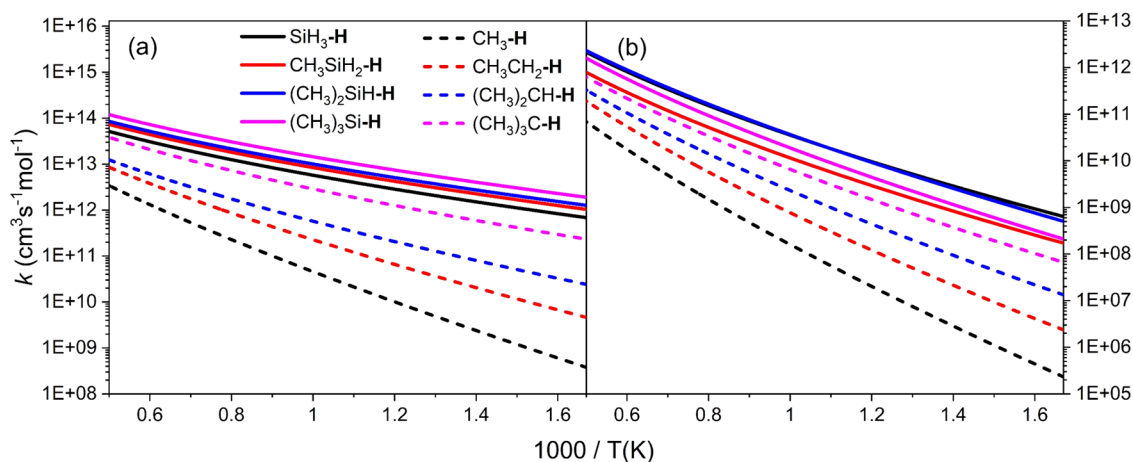

Figure 9. Calculated rate constants of H-abstraction from TeMS and NPT with (a) H attacking and (b) CH_3 attacking at the DLPNO-CCSD(T)/cc-pVTZ//M06−2X/cc-pVTZ level. Black and red solid lines denote the ca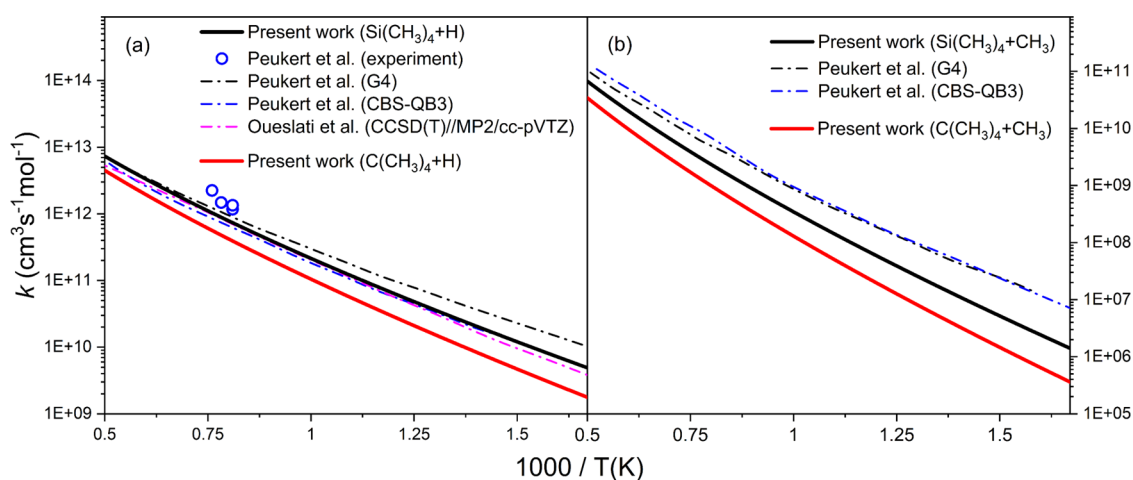lculated results of TeMS and NPT in this work, respectively. Blue hollow circles denote the measured results of TeMS by Peukert et al.[30] Black and blue dashed lines denote the calculated results of TeMS by Peukert et al.[30] at G4 and CBS-QB3 levels, respectively. Purple dashed lines denote the calculated results of TeMS by Oueslati et al.[26] at the CCSD(T)//MP2/cc-pVTZ level.

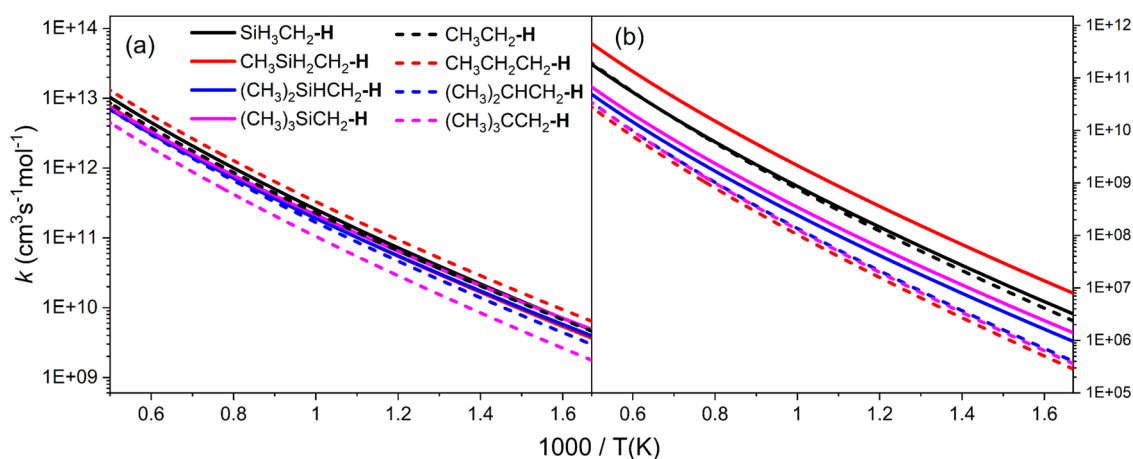abstraction reactions from disilane and ethane. A similar phenomenon can also be observed for k_{11}/k_7 and k_{12}/k_8, which reveals the weak analogy between the H-abstraction reactions from methylsilane and ethane. In contrast, for the H-abstraction reactions from the primary carbon sites in methylsilane and ethane, the rate constants are very close, regardless of which radical attacks. This demonstrates the strong analogy between the H-abstraction reactions from the primary carbon sites, especially compared with the cases of H-abstraction reactions from silicon sites and equivalent carbon sites.

2.2.3. DMS and Propane, TrMS and IBT. The calculated rate constants of H-abstraction reactions from DMS and propane with H attacking (R13, R15, R17, and R19) and CH_3 attacking (R14, R16, R18, and R20) are shown in Figure 6. Figure 6a,c shows that the H-abstraction reactions from the primary carbon sites in DMS and propane have almost parallel rate constants. In more detail, the H-abstraction reaction from the primary carbon site in DMS with H attacking (R13) is about two times slower than that for propane (R17), while that for DMS with CH_3 shown in Figure 6c, the H-abstraction from the H atom in the primary carbon site in DMS by CH_3 is attached to one order

faster than the H-abstraction from propane (R18). The trend that k_{13} is slower than k_{17} while k_{14} is faster than k_{18} is strongly related to that of barrier energies for corresponding reactions, which is described in Section 2.1. As shown in Figure 6b,d, the H-abstraction reactions from the secondary silicon site in DMS with both H and CH_3 attacking are much faster than the H-abstraction reactions from the secondary carbon site in propane, which follows the rule observed in the cases of silane and methane, disilane and ethane, and methylsilane and ethane.

Figure 7a shows that the rate constants of H-abstraction reactions from the primary carbon sites in TrMS (R21) and IBT (R25) with H attacking are close to each other over the investigated temperature region. For the reactions with CH_3 attacking shown in Figure 7c, the rate constant of the reaction for TrMS (R22) is slightly higher than that for IBT (R26), especially under low-temperature conditions. Figure 7b,d shows that the H-abstraction from the tertiary silicon site in TrMS with H attacking (R23) is much faster than that from the tertiary carbon site in IBT (R27), while the discrepancies decrease between the rate constants of the two CH_3 attacking reactions (R24, R28). From the results of the first five cases (silane and

Figure 10. Calculated rate constants of H-abstraction reactions from primary carbon sites in silanes and their alkane counterparts with (a) H attacking and (b) CH_3 attacking.

methane, disilane and ethane, methylsilane and ethane, DMS and propane, and TrMS and IBT), it can be concluded that huge differences exist between the Si atom and C atom, making H-abstraction reactions from silicon sites in silanes cannot be directly referred to similar reactions from equivalent carbon sites in their alkane counterparts.

Figure 8 compares the calculated rate constants of H-abstraction reactions from silicon sites in silanes and equivalent carbon sites in their alkane counterparts. In general, the rate constants of H-abstraction reactions from silicon sites in silanes with H attacking and equivalent carbon sites in their alkane counterparts with H and CH_3 attacking increase as the number of methyl branches increases, which agrees with the decrease of barrier energies shown in Figure 3. In contrast, the rate constants of H-abstraction reactions from silicon sites in silanes with CH_3 attacking have no evident trend with the increasing number of methyl branches. As can be seen from Figure 8b, the rate constants for the four silanes follow the trend of silane $\sim$ DMS > TrMS > methylsilane, while the trend of barrier energies is silane < MS < DMS < TrMS. This discrepancy may come from the influence of entropy caused by the linear configurations of activated complexes in corresponding reactions of silane and methylsilane.

2.2.4. TeMS and NPT. Figure 9 compares the calculated rate constants of H-abstraction reactions from TeMS and NPT with H attacking (R29, R31) and CH_3 attacking (R30, R32), along with measured and calculated results in the literature. Figure 9a shows that the calculated rate constant of H-abstraction from TeMS with H attacking in this work is slightly higher than the calculated results by Oueslati et al.[26] and Peukert et al. at the CBS-QB3 level[30] and lower than the measured results by Peukert et al.[30] and their calculated results at the G4 level,[30] presenting a roughly central location in the distribution of available measured and calculated results. In the present calculated results, the rate constant of H-abstraction from TeMS is around two times higher than that for NPT. For the H-abstraction reactions from TeMS with CH_3 attacking, the present calculated rate constant is lower than the calculated results by Peukert et al.,[30] as shown in Figure 9b. It can also be observed from this figure that the calculated rate constant of H-abstraction from TeMS with CH_3 attacking is about 2−3 times higher than that for NPT over the investigated temperature region.

Figure 10 compares the rate constants of H-abstraction reactions from primary carbon sites in the last four cases (methylsilane and ethane, DMS and propane, TrMS and IBT, and TeMS and NPT). Compared with the situations in Figure 8, relatively strong analogy can be concluded for this kind of reaction between silanes and their alkane counterparts. For methylsilane and ethane, their H-abstraction reactions from primary carbon sites have very close rate constants, regardless of which radical attacks. Similar situation also exists for the H-abstraction reactions from primary carbon sites in TrMS and IBT with H attacking. Under other situations, the H-abstraction reactions from primary carbon sites in TrMS and IBT have generally parallel rate constants, implying that discrepancies mainly exist in pre-exponential factors.

3. CONCLUSIONS

In this work, H-abstraction reactions from silanes (silane, disilane, methylsilane, DMS, TrMS, and TeMS) and their alkane counterparts (methane, ethane, propane, IBT, and NPT) with H and CH_3 attacking were theoretically investigated to reveal differences and similarities between silane systems and alkane systems. Major conclusions are summarized below.

(1) In general, the barrier energies of H-abstraction reactions from silicon sites in silanes are found to be much lower than those from equivalent carbon sites in their alkane counterparts, which are in accordance with the lower BDEs of Si−H bonds than those of equivalent C−H bonds. This can be explained by the different distributions of reactive regions of silanes and their alkane counterparts demonstrated by the different ESP-mapped molecular vdW surfaces.

(2) As the number of methyl branches increases, the barrier energies for H-abstraction reactions from silicon sites in silanes with CH_3 attacking and equivalent carbon sites in their alkane counterparts with H and CH_3 attacking follow the trends of corresponding BDEs, which results in only slightly lower barrier energy of H-abstraction from the tertiary silicon site in TrMS with CH_3 attacking than that from the equivalent carbon site in IBT. Exceptionally, the barrier energies for H-abstraction reactions from silicon sites in silanes with H attacking do not follow the trend of corresponding BDEs due to the increasing nucleophilic capacity of H atom on the silicon sites.

(3) The H-abstraction reactions from the primary carbon sites in silanes have generally lower barrier energies than the similar reactions in their alkane counterparts, while those in methylsilane and DMS with H attacking are the only two with higher barrier energies. The two exceptions are mainly caused by the relatively difficult H attacking on the primary carbon sites in methylsilane and DMS due to their relatively large and strong electron-affinitive regions in the primary carbon sites and small electronegative regions.

(4) In general, the rate constants of H-abstraction reactions from silicon sites in silanes with H attacking and equivalent carbon sites in their alkane counterparts with H and CH_3 attacking increase as the number of methyl branches increases, which agrees with the decrease of barrier energies. In contrast, the rate constants of H-abstraction reactions from silicon sites in silanes with CH_3 attacking have no evident trend. The H-abstraction reactions from silicon sites in silanes have much higher rate constants than those from equivalent carbon sites in their alkane counterparts, while the discrepancies become generally greater as the temperature decreases, except for the case of TrMS and IBT with CH_3 attacking.

(5) Compared with the H-abstraction reactions from silicon sites and equivalent carbon sites, the rate constants of H-abstraction reactions from primary carbon sites in silanes and their alkane counterparts show relatively strong analogy, especially for the situations of methylsilane and ethane with H and CH_3 attacking and TrMS and IBT with H attacking.

4. COMPUTATIONAL DETAILS

Geometries and frequencies were calculated employing the density functional theory (DFT) method M06−2X[34] with the cc-pVTZ basis set.[35] A frequency scaling factor of 0.948 was used to correct zero-point energy (ZPE).[36] To facilitate the calculation of TeMS and NPT with five heavy atoms, the domain-based local pair natural orbital coupled cluster with perturbative triple excitations (DLPNO-CCSD(T)) method proposed by Liakos et al.[37] was employed in the single-point energy (SPE) calculation. This method can evaluate coupled cluster energy with higher efficiency at less time and accuracy costs,[38] has an uncertainty of about 0.5 kcal/mol compared with the standard CCSD(T) method,[37] and has been widely applied in SPE calculations of systems with similar sizes.[39−42] Many benchmark datasets show that this method can provide approximately the same accuracy and reliability as the current standard CCSD(T) method.[43,44] For open shells, the accuracy of the DLPNO calculations can be significantly improved through an iterative version of the triples correction method.[44,45] Subhasish et al.[46] assessed the accuracy of the DLPNO-CCSD(T) method against the CCSD(T) method in determining the barrier heights and reaction energetics for a series of hydrogen atom transfer reactions and suggested the standard deviation for the open-shell systems as 0.79 kcal/mol (within 1 kcal/mol). Among the three truncation thresholds (TightPNO, NormalPNO, and LoosePNO) in the DLPNO-CCSD(T) method, the first one with the highest calculation accuracy was adopted in this work following the setting adopted in the work of Sun et al.[47] All of the quantum chemical calculations, including geometry optimization, frequency analysis, and relaxed scan were performed using the Gaussian 09 program.[48] The SPEs

were computed using the ORCA 4.2.1 program.[49] Furthermore, the ESP-mapped molecular vdW surfaces were also calculated based on the wavefunction analyses using the Multiwfn 3.8 code[50] to provide insight into the differences and similarities in H-abstraction barrier energies between silanes and their alkane counterparts. The wavefunctions used in the ESP analyses were calculated at the M06−2X/cc-pVTZ level. All isosurface maps were generated based on the outputs of Multiwfn using the VMD 1.9.3 program.[50,51]

In this paper, the rate constants of H-abstraction reactions were calculated using conventional transition state theory (CTST), which was implemented in the KiSThelP code.[52] Conventional TST calculations only require information of the saddle points and reactants. The rate constant of a bimolecular reaction is described by the following equation

$$k^{TST} = \sigma \frac{k_b T}{h} \frac{Q^{TS}(T)}{N_A Q^R(T)} e^{(-V^*/k_b T)}$$

where σ is the reaction path degeneracy, k_b is Boltzmann constant, T is the temperature, h is Planck constant, N_A is Avogadro number, V^* is the difference in zero-point excluded potential energy between transition states (TSs) and reactants, Q_{TS} and Q_R denote the total partition functions of the TS and reactants with the translational partition functions expressed in per unit volume.

The one-dimensional asymmetric Eckart correction was applied to account for tunneling. Low-frequency internal rotations of CH_3 groups were treated as hindered rotations using the hindered rotor density of states (HRDS) method,[53] which is implemented in the KiSThelP program. The rotational barrier energies were obtained through CH_3 scanning at an interval of $10°$ at the same level of theory as optimization and frequency calculation. As shown in Figure S1, it can be found that the rotational barrier energies are similar between the CH_3 groups of methylsilane, DMS, TrMS, and TeMS, which are lower than those of their alkane counterparts.

In this work, the rate constants of all reactions were obtained per H atom, while some measured and calculated results in the literature, which are per molecule or per site, were also converted to be per H atom for comparison. To verify the rationality of the chosen calculation method, the calculated rate constants for H-abstraction reactions from methane, ethane, propane, and NPT with H and CH_3 attacking were compared with previously measured and calculated results in the literature. As shown in Figures S2−S6 in the Supporting Information, it can be found that the calculated results in this work are generally in good agreement with previously measured and calculated results.

■ ASSOCIATED CONTENT

🅢 Supporting Information

The Supporting Information is available free of charge at https://pubs.acs.org/doi/10.1021/acsomega.1c07031.

> Hindrance potentials of the CH_3 rotors for methylsilane, DMS, TrMS, TeMS, ethane, propane, IBT, and NPT; comparison of calculated rate constants for H-abstraction reactions from methane, ethane, propane, and NPT with H and CH_3 attacking with previously measured and calculated results in the literature; configuration and ESP-mapped molecular vdW surface of CH_3 radical (S1); potential energy surfaces (PESs) (S2); relative enthalpies, free energies and entropies of the H-abstraction (S3); and

geometries and frequencies of reactants and transition states (TSs) (S4) (PDF)

AUTHOR INFORMATION

Corresponding Author

Yuyang Li − *Key Laboratory for Power Machinery and Engineering of MOE, School of Mechanical Engineering, Shanghai Jiao Tong University, Shanghai 200240, P. R. China;* ⊙ orcid.org/0000-0002-0900-9234; Email: yuygli@sjtu.edu.cn

Authors

Qilong Fang − *Key Laboratory for Power Machinery and Engineering of MOE, School of Mechanical Engineering, Shanghai Jiao Tong University, Shanghai 200240, P. R. China*

Yan Zhang − *Key Laboratory for Power Machinery and Engineering of MOE, School of Mechanical Engineering, Shanghai Jiao Tong University, Shanghai 200240, P. R. China*

Jingxian Xia − *Key Laboratory for Power Machinery and Engineering of MOE, School of Mechanical Engineering, Shanghai Jiao Tong University, Shanghai 200240, P. R. China*

Complete contact information is available at:
https://pubs.acs.org/10.1021/acsomega.1c07031

Notes

The authors declare no competing financial interest.

ACKNOWLEDGMENTS

REFERENCES

(1) Ma, Z. H.; Tian, H.; Cong, L. Y.; Wu, Q.; Yue, M.; Sun, S. H. A flame-reaction method for the large-scale synthesis of high-performance Sm$_x$Co$_y$ nanomagnets. *Angew. Chem., Int. Ed.* **2019**, *58*, 14509−14512.

(2) Zong, Y. C.; Li, S. Q.; Niu, F.; Yao, Q. Direct synthesis of supported palladium catalysts for methane combustion by stagnation swirl flame. *Proc. Combust. Inst.* **2015**, *35*, 2249−2257.

(3) Hong, H.; Memon, N. K.; Dong, Z. Z.; Kear, B. H.; Tse, S. D. Flame synthesis of gamma-iron-oxide (γ-Fe$_2$O$_3$) nanocrystal films and carbon nanotubes on stainless-steel substrates. *Proc. Combust. Inst.* **2019**, *37*, 1249−1256.

(4) Tian, A. X.; Wang, L. Q.; Wang, N. F.; Wang, S. H.; Cai, J. Z.; Huang, Q.; Huang, Y. Palladium-based catalysts for methane oxidation by co-flow diffusion flame synthesis. *Powder Technol.* **2019**, *354*, 402−409.

(5) Zhao, N.; Gao, M. Y. Magnetic janus particles prepared by a flame synthetic approach: Synthesis, characterizations and properties. *Adv. Mater.* **2009**, *21*, 184−187.

(6) Meierhofer, F.; Fritsching, U. Synthesis of metal oxide nanoparticles in flame sprays: Review on process technology, modeling, and diagnostics. *Energy Fuels* **2021**, *35*, 5495−5537.

(7) Gutsch, A.; Krämer, M.; Michael, G.; Mühlenweg, H.; Pridöhl, M.; Zimmermann, G. Gas-phase production of nanoparticles. *KONA Powder Part. J.* **2002**, *20*, 24−37.

(8) Wei, J.; Li, S.; Ren, Y.; Zhang, Y.; Tse, S. D. Investigating the role of solvent formulations in temperature-controlled liquid-fed aerosol flame synthesis of YAG-based nanoparticles. *Proc. Combust. Inst.* **2019**, *37*, 1193−1201.

(9) Wu, Z. Y.; Zhang, Y. Y.; Zhao, X. F.; Wang, H. Y.; Li, S. Q. Dual liquid/vapor-fed flame synthesis for the effective preparation of SiO$_2$@

YAlO$_3$: Nd^{3+} nanophosphors. *Proc. Combust. Inst.* **2021**, *38*, 1299−1307.

(10) Okada, S.; Sugime, H.; Hasegawa, K.; Osawa, T.; Kataoka, S.; Sugiura, H.; Noda, S. Flame-assisted chemical vapor deposition for continuous gas-phase synthesis of 1-nm-diameter single-wall carbon nanotubes. *Carbon* **2018**, *138*, 1−7.

(11) Li, S. Q.; Ren, Y. H.; Biswas, P.; Tse, S. D. Flame aerosol synthesis of nanostructured materials and functional devices: Processing, modeling, and diagnostics. *Prog. Energy Combust. Sci.* **2016**, *55*, 1−59.

(12) Schulz, C.; Dreier, T.; Fikri, M.; Wiggers, H. Gas-phase synthesis of functional nanomaterials: Challenges to kinetics, diagnostics, and process development. *Proc. Combust. Inst.* **2019**, *37*, 83−108.

(13) Britten, J. A.; Tong, J.; Westbrook, C. K. A numerical study of silane combustion. *Symp. (Int.) Combust.* **1991**, *23*, 195−202.

(14) Miller, T. A.; Wooldridge, M. S.; Bozzelli, J. W. Computational modeling of the SiH$_3$+O$_2$ reaction and silane combustion. *Combust. Flame* **2004**, *137*, 73−92.

(15) Parandaman, A.; Rajakumar, B. Kinetics of the thermal decomposition of tetramethylsilane behind the reflected shock waves between 1058 and 1194 K. *J. Chem. Sci.* **2016**, *128*, 573−588.

(16) Sela, P.; Peukert, S.; Herzler, J.; Fikri, M.; Schulz, C. Shock-tube study of the decomposition of tetramethylsilane using gas chromatography and high-repetition-rate time-of-flight mass spectrometry. *Phys. Chem. Chem. Phys.* **2018**, *20*, 10686−10696.

(17) Janbazi, H.; Karakaya, Y.; Kasper, T.; Schulz, C.; Wlokas, I.; Peukert, S. Development and evaluation of a chemical kinetics reaction mechanism for tetramethylsilane-doped flames. *Chem. Eng. Sci.* **2019**, *209*, 115209−115224.

(18) Zhang, Y.; Xia, J.; Fang, Q.; Li, Y. Comparative investigation on tetramethylsilane and neopentane combustion: Jet-stirred reactor pyrolysis and kinetic modeling. *Combust. Flame* **2022**, *237*, 111900−111909.

(19) Mick, H. J.; Markus, M. W.; Roth, P.; Smirnov, V. N. A shock tube study of the thermal decomposition of Si$_2$H$_6$ based on Si and SiH$_2$ measurements. *Ber. Bunsenges. Phys. Chem.* **1995**, *99*, 880−890.

(20) Quandt, R. W.; Hershberger, J. F. Kinetics of the SiH$_3$ + O$_2$ and SiH$_3$ + NO$_2$ reactions. *Chem. Phys. Lett.* **1993**, *206*, 355−360.

(21) Meyer, J. P.; Hershberger, J. F. Kinetics of the SiH$_3$ + H$_2$O$_2$ and SiH$_3$ + O$_2$ Reactions. *J. Phys. Chem. A* **2003**, *107*, 5963−5967.

(22) Ding, L.; Marshall, P. Does alkyl substitution affect the silicon-hydrogen bond strength in silane? Kinetic studies of the reactions of atomic chlorine and bromine with trimethylsilane and an ab initio investigation. *J. Am. Chem. Soc.* **1992**, *114*, 5754−5758.

(23) Espinosa-García, J.; Sansón, J.; Corchado, J. C. The SiH$_4$+H→ SiH$_3$+H$_2$ reaction: Potential energy surface, rate constants, and kinetic isotope effects. *J. Chem. Phys.* **1998**, *109*, 466−473.

(24) Wu, S. Y.; Raghunath, P.; Wu, J. S.; Lin, M. C. Ab initio chemical kinetic study for reactions of H atoms with SiH$_4$ and Si$_2$H$_6$: Comparison of theory and experiment. *J. Phys. Chem. A* **2010**, *114*, 633−639.

(25) Qi, C. S.; Sun, X. M. Theoretical studies of the reaction paths and rate constants for SiH$_4$ + H system. *Asian J. Chem.* **2012**, *24*, 1798−1804.

(26) Oueslati, I.; Kerkeni, B.; Spielfiedel, A.; Tchang-Brillet, W. U.; Feautrier, N. Ab initio investigation of the abstraction reactions by H and D from tetramethylsilane and its deuterated substitutions. *J. Phys. Chem. A* **2014**, *118*, 791−802.

(27) Sela, P.; Peukert, S.; Herzler, J.; Sakai, Y.; Fikri, M.; Schulz, C. High-temperature gas-phase kinetics of the thermal decomposition of tetramethoxysilane. *Proc. Combust. Inst.* **2019**, *37*, 1133−1141.

(28) Nurkowski, D.; Buerger, P.; Akroyd, J.; Kraft, M. A detailed kinetic study of the thermal decomposition of tetraethoxysilane. *Proc. Combust. Inst.* **2015**, *35*, 2291−2298.

(29) Nurkowski, D.; Buerger, P.; Akroyd, J.; Mosbach, S.; Kraft, M. Skeletal chemical mechanism of high-temperature TEOS oxidation in hydrogen-oxygen environment. *Combust. Flame* **2016**, *166*, 243−254.

(30) Peukert, S.; Herzler, J.; Fikri, M.; Schulz, C. High-temperature rate constants for H + tetramethylsilane and H + silane and implications about structure-activity relationships for silanes. *Int. J. Chem. Kinet.* **2018**, *50*, 57−72.

(31) Peukert, S.; Yatsenko, P.; Fikri, M.; Schulz, C. High-temperature rate constants for the reaction of hydrogen atoms with tetramethoxysilane and reactivity analogies between silanes and oxygenated hydrocarbons. *J. Phys. Chem. A* **2018**, *122*, 5289–5298.

(32) Nurkowski, D.; Klippenstein, S. J.; Georgievskii, Y.; Verdicchio, M.; Jasper, A. W.; Akroyd, J.; Mosbach, S.; Kraft, M. Ab initio variational transition state theory and master equation study of the reaction $(OH)_3SiOCH_2 + CH_3 \rightleftharpoons (OH)_3SiOC_2H_5$. *Z. Phys. Chem.* **2015**, *229*, 691–708.

(33) Luo, Y. R. *Comprehensive Handbook of Chemical Bond Energies*; CRC Press, 2007.

(34) Zhao, Y.; Truhlar, D. G. The M06 suite of density functionals for main group thermochemistry, thermochemical kinetics, noncovalent interactions, excited states, and transition elements: Two new functionals and systematic testing of four M06-class functionals and 12 other functionals. *Theor. Chem. Acc.* **2008**, *120*, 215–241.

(35) Dunning, T. H. Gaussian basis sets for use in correlated molecular calculations. I. The atoms boron through neon and hydrogen. *J. Chem. Phys.* **1989**, *90*, 1007–1023.

(36) Kashinski, D. O.; Chase, G. M.; Nelson, R. G.; Di Nallo, O. E.; Scales, A. N.; VanderLey, D. L.; Byrd, E. F. Harmonic vibrational frequencies: Approximate global scaling factors for TPSS, M06, and M11 functional families using several common basis sets. *J. Phys. Chem. A* **2017**, *121*, 2265–2273.

(37) Liakos, D. G.; Neese, F. Is it possible to obtain coupled cluster quality energies at near density functional theory cost? Domain-based local pair natural orbital coupled cluster vs modern density functional theory. *J. Chem. Theory Comput.* **2015**, *11*, 4054–4063.

(38) Zhao, Q.; Zhang, Y. J.; Zhang, F.; Huang, Z. H. Pressure-dependent kinetics on benzoyl radical + O_2 and its implications for low temperature oxidation of benzaldehyde. *Combust. Flame* **2020**, *214*, 139–151.

(39) Kröger, L. C.; Döntgen, M.; Firaha, D.; Kopp, W. A.; Leonhard, K. Ab initio kinetics predictions for H-atom abstraction from diethoxymethane by hydrogen, methyl, and ethyl radicals and the subsequent unimolecular reactions. *Proc. Combust. Inst.* **2019**, *37*, 275–282.

(40) Yin, G. Y.; Gao, Z. H.; Hu, E. J.; Xu, Z. H.; Huang, Z. H. Comprehensive experimental and kinetic study of 2,4,4-trimethyl-1-pentene oxidation. *Combust. Flame* **2019**, *208*, 246–261.

(41) Yang, F. Y.; Zhang, Y. J.; Sun, W. C.; Zhao, Q.; Huang, W. L.; Qin, X. K.; Deng, F. Q.; Huang, Z. H. Theoretical kinetics of hydrogen abstraction and addition reactions of 3-hexene by Ḣ, Ö(3P) and ĊH₃. *Combust. Flame* **2018**, *197*, 449–462.

(42) Li, W.; Cao, C.; Zhang, X.; Li, Y.; Yang, J.; Zou, J.; Mei, B.; Cheng, Z. Exploring combustion chemistry of ethyl valerate at various pressures: Pyrolysis, laminar burning velocity and kinetic modeling. *Combust. Flame* **2021**, *227*, 27–38.

(43) Koerstz, M.; Elm, J.; Mikkelsen, K. V. Benchmark study of the structural and thermochemical properties of a dihydroazulene/vinylheptafulvene photoswitch. *J. Phys. Chem. A* **2017**, *121*, 3148–3154.

(44) Liakos, D. G.; Guo, Y.; Neese, F. Comprehensive benchmark results for the domain based local pair natural orbital coupled cluster method (DLPNO-CCSD(T)) for closed- and open-shell systems. *J. Phys. Chem. A* **2020**, *124*, 90–100.

(45) Guo, Y.; Riplinger, C.; Becker, U.; Liakos, D. G.; Minenkov, Y.; Cavallo, L.; Neese, F. Communication: An improved linear scaling perturbative triples correction for the domain based local pair-natural orbital based singles and doubles coupled cluster method [DLPNO-CCSD(T)]. *J. Chem. Phys.* **2018**, *148*, No. 011101.

(46) Mallick, S.; Roy, B.; Kumar, P. A comparison of DLPNO-CCSD(T) and CCSD(T) method for the determination of the energetics of hydrogen atom transfer reactions. *Comput. Theor. Chem.* **2020**, *1187*, 112934–112944.

(47) Sun, Y. J.; Somers, K. P.; Wang, Q. D.; Farrell, C.; Curran, H. J. Hindered rotor benchmarks for the transition states of free radical additions to unsaturated hydrocarbons. *Phys. Chem. Chem. Phys.* **2020**, *22*, 27241–27254.

(48) Frisch, M. J.; Trucks, G. W.; Schlegel, H. B.; Scuseria, G. E.; Robb, M. A.; Cheeseman, J. R.; Scalmani, G.; Barone, V.; Petersson, G. A.; Nakatsuji, H.; Li, X.; Caricato, M.; Marenich, A. V.; Bloino, J.; Janesko, B. G.; Gomperts, R.; Mennucci, B.; Hratchian, H. P.; Ortiz, J. V.; Izmaylov, A. F.; Sonnenberg, J. L.; Williams; Ding, F.; Lipparini, F.; Egidi, F.; Goings, J.; Peng, B.; Petrone, A.; Henderson, T.; Ranasinghe, D.; Zakrzewski, V. G.; Gao, J.; Rega, N.; Zheng, G.; Liang, W.; Hada, M.; Ehara, M.; Toyota, K.; Fukuda, R.; Hasegawa, J.; Ishida, M.; Nakajima, T.; Honda, Y.; Kitao, O.; Nakai, H.; Vreven, T.; Throssell, K.; Montgomery, J. A., Jr.; Peralta, J. E.; Ogliaro, F.; Bearpark, M. J.; Heyd, J. J.; Brothers, E. N.; Kudin, K. N.; Staroverov, V. N.; Keith, T. A.; Kobayashi, R.; Normand, J.; Raghavachari, K.; Rendell, A. P.; Burant, J. C.; Iyengar, S. S.; Tomasi, J.; Cossi, M.; Millam, J. M.; Klene, M.; Adamo, C.; Cammi, R.; Ochterski, J. W.; Martin, R. L.; Morokuma, K.; Farkas, O.; Foresman, J. B.; Fox, D. J. *Gaussian 09*, Rev. A.02; Gaussian, Inc.: Wallingford, CT, 2016.

(49) Neese, F. The ORCA program system. *Wiley Interdiscip. Rev.: Comput. Mol. Sci.* **2012**, *2*, 73–78.

(50) Lu, T.; Chen, F. W. Multiwfn: A multifunctional wavefunction analyzer. *J. Comput. Chem.* **2012**, *33*, 580–592.

(51) Humphrey, W.; Dalke, A.; Schulten, K. VMD: Visual molecular dynamics. *J. Mol. Graphics* **1996**, *14*, 33–38.

(52) Canneaux, S.; Bohr, F.; Henon, E. KiSThelP: A program to predict thermodynamic properties and rate constants from quantum chemistry results. *J. Comput. Chem.* **2014**, *35*, 82–93.

(53) McClurg, R. B.; Flagan, R. C.; Goddard, W. A., III The hindered rotor density-of-states interpolation function. *J. Chem. Phys.* **1997**, *106*, 6675–6680.